ACS OMEGA

http://pubs.acs.org/journal/acsodf

Article

Cross-Linked Chitosan/Gelatin Beads Loaded with *Chlorella vulgaris* Microalgae/Zinc Oxide Nanoparticles for Adsorbing Carcinogenic Bisphenol-A Pollutant from Water

Hazim M. Ali,[†] Omar M. Ibrahim,[†] Ahmed S. M. Ali, Mahmoud A. Mohamed, Rehab Y. Ghareeb, Elsayed E. Hafez, and Mohamed R. El-Aassar*

Cite This: *ACS Omega* 2022, 7, 27239−27248

Read Online

ACCESS | Metrics & More | Article Recommendations | Supporting Information

ABSTRACT: Water polluted by phenolic compounds is a global threat to health and the environment; accordingly, we prepared a green novel sorbent biological system from a chitosan (CS), gelatin (GT), and *Chlorella vulgaris* freshwater microalgae (m-Alg) composite impregnated with zinc oxide nanoparticles (ZnO-NPs) for the remediation of bisphenol-A (BPA) from water. *C. vulgaris* was selected to be one of the constituents of the prepared composite because of its high capability in phytoremediation. The morphology and the structure of CS/GT*m-Alg/ZnO beads were characterized by SEM, FTIR, XRD, and TGA. Different monitoring experimental conditions, such as contact time, pH, BPA concentration, and sorbent dosage, were optimized. The optimum conditions for the adsorption process showed outstanding removal efficiency toward BPA at pH 4.0, contact time 40.0 min, and 40.0 mg L^{-1} BPA initial concentration. Langmuir, Freundlich, and Temkin isotherm models have been studied for adsorption equilibrium, and the best fit is described by the Langmuir adsorption isotherm. The adsorption kinetics has been studied using pseudo-first-order (PFO), pseudo-second-order (PSO), Elovich, and intraparticle diffusion (IPD) models. The pseudo-second-order kinetic model shows the optimum experimental fit. The monolayer adsorption capacity of the prepared CS/GT*m-Alg/ZnO for BPA was determined to be 38.24 mg g^{-1}. The prepared CS/GT*m-Alg/ZnO beads show advantageous properties, such as their high surface area, high adsorption capacity, reusability, and cost-effectiveness.

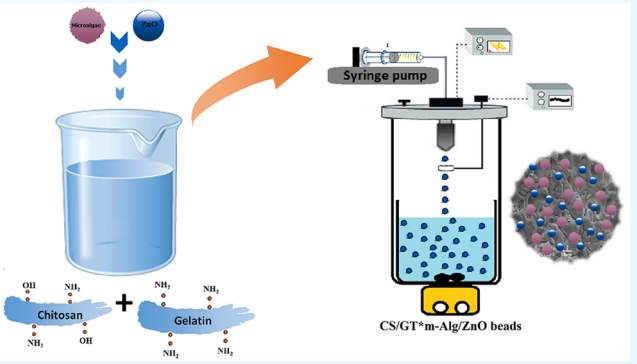

1. INTRODUCTION

Endocrine disrupting chemicals (EDCs) are the main components in many synthetic products because of their wide range of usage and growing demand, and this has been a reason for environmental concern globally.[1] EDC artificial compounds adversely disturb the endocrine system, leading to neurological, reproductive, and developmental systems' health related problems.[2] EDCs are included in many products that are used daily, such as lotions, shampoos, and shaving creams. EDCs are emerging as a threatening contamination source for aquatic environments.[3] Therefore, EDC pollutants are a threat to human and animal health and the environment, and they should be cleansed from aqueous solution to avoid their severe health problems,[4] including cancer.[5,6] Bisphenol-A (BPA) is an example of an EDC. BPA is mainly used in the manufacturing of polycarbonates and epoxy resins.[7,8] Also, it is used in thermal papers, can coatings, powder paints, dental fillings, and plastics.[9,10] BPA is identified as an endocrine disrupting chemical. To dispose such harmful compounds, advanced oxidation processes such as the Fenton reaction,[11] ozonation,[12] photocatalytic oxidation, and ultrasonic oxidation[13] have been developed to oxidize and dispose of harmful phenolic compounds leading to the generation of hydroxyl radicals [$OH^{\bullet}$].[14−16] However, these technologies are time and money consuming and produce toxic byproducts.[8] On the other hand, adsorption[17,18] is superior for removal of phenolic compounds due to its fast and convenient screening out of toxic phenolic contaminants,[8] in addition to its low initial costs and trouble-free design.[19]

Materials based polymers are the most common adsorbents that are known for their functionality toward BPA removal processes.[17,18] Recently, chitosan (CT) has been used as an idealistic green adsorbent for disposal of phenolic pollutants. Also, CT has relatively low cost and high adsorption capacity

Received: March 31, 2022
Accepted: July 7, 2022
Published: July 26, 2022

for BPA removal.[20,21] CT is a plentiful biopolymer produced from chitin using fungal species.[22] Due to the low surface area, high crystallinity, resistance to mass transfer, low porosity, and low adsorption capability of CT adsorbent in the form of flakes, its applications are limited.[22] To overcome these problems, CT could be physically modified via conversion to achieve favorable properties and applications of its derivatives. Such modifications would boost the porosity, polymer chains, available surface area, and access to internal adsorption sites and decrease the crystallinity, leading to better adsorption capacity.[23] The overall physical and mechanical properties of CT can be enhanced upon blending with other polymers such as gelatin. Both CT and gelatin are biodegradable, biocompatible, and ecofriendly polymers, and their blends yield enhanced overall physical and mechanical properties upon cross-linking.[24,25,7,26]

Yan et al. has shown superior elimination of BPA upon adding zinc oxide.[27] In recent years, the use of zinc oxide nanoparticles (ZnO-NPs) with such optimized properties and functions has been investigated due to their nano size range and large surface area to volume ratios.[28] All of these points make ZnO an ideal component for elimination of bisphenol-A.

Microalgae have the ability to eliminate water pollutants such as phenol, heavy metals, herbicides, and hexachlorobenzene.[29] Also, it has been reported that algae have the capabilities for the biodegradation of environmental organic impurities.[29,30] Hirooka et al. have reported the superior ability of *Chlorella fusca* algae in the elimination of bisphenol-A,[31] indicating that microalgae can eliminate contaminants from wastewater and can be effective in waste treatment facilities.

Since BPA is a threat to human health and to the environment, the main theme of this work is to develop a new biological system to eliminate the BPA environmental threat. In order to enhance the adsorption capacity of the adsorbent, cross-linked chitosan/gelatin beads loaded with microalgae/zinc oxide nanoparticles were fabricated. To gain an understanding of the adsorption mechanism, the different fabricated sorbents were characterized by SEM, FT-IR, XRD, and TGA techniques. The adsorption capacity for each sorbent toward remediation of BPA was also investigated. The equilibrium data were modeled using linear isotherm and kinetics equations. Herein, we report an economic and easily applicable material for BPA disposable. The results show that the adsorption efficiency of chitosan toward BPA was improved by the incorporation of ZnO-NPs and microalgae.

2. EXPERIMENTAL SECTION

2.1. Materials. Gelatin (GT, isoelectric point of 5, M_w 40−50 kDa), chitosan (CT, degree of deacetylation (DD) 88%), and zinc acetate ($Zn(CH_3COO)_2{\cdot}2H_2O$, 99.5%) were obtained from Sigma-Aldrich Chemicals Ltd. (Schnelldorf, Germany). Bisphenol-A (BPA, $C_{15}H_{16}O_2$, FW 228.29 g/mol and assay >99%) was obtained from Dr. Ehrenstorfer GmbH (Augsburg, Germany), and dichloromethane (DCM, CH_2Cl_2, purity ≥99%) and *n*-hexane (C_6H_{14}, purity ≥99%) were obtained from Dr. Carl Roth GmbH (Karlsruhe, Germany). All other chemicals were of analytical grade.

2.2. Microalgae Strain, Cultivation, and Biomass. 100 mL of Bold's Basal Medium (BBM)[31] in a 250 mL Erlenmeyer flask was inoculated with the pure culture cells of green microalgae *Chlorella vulgaris* (OD_{680} 0.05) under GeneBank accession number FR751187, and the culture was incubated at 27 ± 2 °C with 150 rpm shaking under continuous illumination of 45−50 μmol photon m^{-2} s^{-1} white fluorescent light for 21 day. Microalgae were harvested by centrifugation at 8000*g* and washed with water. Microalgae pellets were dried at 50 °C overnight to be used in the following experiments. 1 mg (8 × 108) was added to the chitosan/gelatin solution.

2.3. Preparation of Zinc Oxide Nanoparticles (ZnO-NPs). 2 M sodium hydroxide was added dropwise to a 1 M zinc acetate solution and kept under stirring until the generation of a white slurry. After 20 h of stirring, the resulting white precipitate was filtered off and washed, followed by furnace drying and grinding into a fine powder that was calcined at 400 °C.[32]

2.4. Fabrication of Sorbent Beads. *Step 1* was to prepare a 2% chitosan solution by dissolving 2 g of chitosan in 100 mL of 2% acetic acid at room temperature and prepare a 0.25% gelatin solution at 50 °C.

Step 2 was to mix both solutions together and stir for 1 h at 50 °C to obtain a homogeneous solution.

Step 3 was to pour equal volumes from polymer solutions into three beakers and load with ZnO-NPs, algae, or ZnO-NPs and algae together.

Step 4: for preparation of beads, 10 mL of the latest solution was poured into a stirring salt solution composing of 100 mL of 3% (w/v) NaOH as cross-linker using a 100 μL spray nozzle and stirred for 30 min. The resultant beads were filtered and washed with distilled water.

2.5. Characterization. The size and structure of the CS/GT*m-Alg/ZnO microsphere beads were characterized with a scanning electron microscope (JEOL, JSM-6610LV, Japan). Powder XRD (Shimadzu XRD-7000, Japan) demonstrated the XRD pattern of the sorbent materials. The fabricated CS/GT*m-Alg/ZnO beads were confirmed by FT-IR (Shimadzu FTIR-8400 S, Japan). The effect of ZnO-NPs and algae impregnation on the thermal stability was determined with a thermogravimetric analyzer (TGA, Shimadzu TGA-50, Japan).[33,34]

The BPA in the samples after adsorption was detected by a gas chromatographer equipped with an HP-5MS UI column (30 m length, 0.25 mm internal diameter, and 0.25 μm film thicknesses) coupled to a quadrupole mass detector (GC-MS system, Agilent Technologies 7890A-5975C, USA).

2.6. Adsorption Procedure. To prepare the experimental solutions, stock solutions of BPA were prepared by liquifying BPA in DCM. The solution was diluted to obtain a standard solution of 10−60 mg L^{-1}. 0.05−0.25 g quantities of different sorbents were added at pH values (2−9) adjusted by HCl or NaOH. The solution was agitated in a shaker (140 rpm) at different contact times (0−60 min), and the adsorbent was centrifuged. The amount of BPA present in the solution was detected by using GC-MS, and the removal percentage (% Removal) of BPA can be calculated by eq 1

$$\%\text{Removal} = \frac{(C_0 - C_e)}{C_0} \times 100 \tag{1}$$

where C_0 is the initial BPA concentration (mg L^{-1}) and C_e is the BPA concentration at equilibrium (mg L^{-1}). Also, the adsorption efficiency at equilibrium was determined by eq 2

$$q_e = \left(\frac{C_0 - C_e}{W}\right)v \tag{2}$$

https://doi.org/10.1021/acsomega.2c01985
ACS Omega 2022, 7, 27239−27248

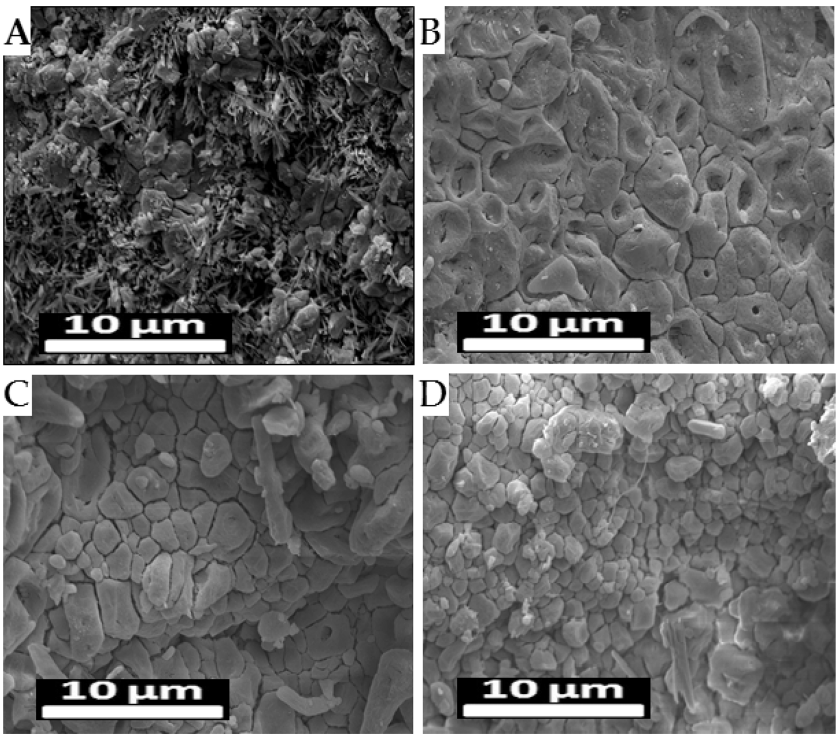

Figure 1. SEM images of (A) CS/GT, (B) CS/GT/ZnO, (C) CS/GT*m-Alg, and (D) CS/GT*m-Alg/ZnO beads.

where q_e is the adsorbed amount of BPA onto different adsorbents (mg g^{-1}), w is the weight of adsorbent (g), and v is the volume of BPA solution (L).

The kinetic adsorption efficiency was investigated upon the contact of certain amounts of adsorbents with BPA solutions of different initial concentrations at 25 ± 1°C. The adsorption performance was estimated by eq 3

$$q_t = \left(\frac{C_0 - C_t}{W}\right)v \quad (3)$$

where q_t is the adsorption capacity at time t (mg g^{-1}) and C_t is the BPA concentration at time t (mg L^{-1}).

2.7. Sample Preparation for GC-MS. Diluted samples (10−100) were injected into a GC-MS instrument. All the experiments were performed in at least duplicate to guarantee the reliability and reproducibility of the data. The data reproducibility was within 4%. Supplementary Figure 1 shows the GC chromatogram of BPA removal.

3. RESULTS AND DISCUSSION

3.1. Characterization of the Prepared Hydrogels. *3.1.1. SEM Analysis.* Figure 1 shows a representative SEM image of the composites obtained. The figure shows that the CS*/GT composite has an irregular surface and various pore sizes. Also, the morphologies of the CS/GT/ZnO, CS/GT*m-Alg, and CS/GT*m-Alg/ZnO composites do not resemble the morphology of CS/GT. Figure 1C and D confirms the uniform morphological structure and well-developed external macroporosity of the generated CS/GT*m-Alg and CS/GT*m-Alg/ZnO beads, suggesting successful generation of uniform beads.

3.1.2. FTIR Analysis. In Figure 2A, the spectra of CS/GT*m-Alg/ZnO beads show the peaks of C−O−C at 1028 cm^{-1}, C−OH at 1436 cm^{-1}, C═O at 1644 cm^{-1}, C−H at 2926 cm^{-1}, and C−H and N−H at 3440 cm^{-1}. The enhanced transmittance signals of CS/GT*m-Alg/ZnO at 1644 and 1028 cm^{-1} might be due to the lipid and carbohydrate components, respectively, of the algae.[35] These confirm the presence of the C−O−C, C−OH, C═O, C−H, and N−H major chemical groups of the used composite components without observed chemical interaction or newer peaks.[25,24]

3.1.3. XRD Analysis. The X-ray diffraction patterns of CS/GT, CS/GT/ZnO, and CS/GT*m-Alg/ZnO beads are illustrated in Figure 2B. In general, two main forms of ZnO crystals are found: cubic zinc blende and hexagonal wurtzite.[36] It was reported that the crystal wurtzite form is the most stable structure at ambient conditions.[37] Figure 2B displays peaks at the 2θ values 31.25°, 34.46°, 36.18°, 47.44°, 56.26°, 63.46°, 68.22°, and 69.58° in CS/GT/ZnO and CS/GT*m-Alg/ZnO beads but not in CS/GT blank beads. All characteristic peaks could be indexed as the ZnO-NPs present as the wurtzite structure (JCPDS Data Card No: 36-1451). These confirm the successful incorporation of ZnO-NPs in the fabricated beads.

3.1.4. TGA Analysis. Figure 2C shows the thermal decomposition of CS/GT, CS/GT/ZnO, and CS/GT*m-Alg/ZnO beads. It is obvious from the figure that the modified CS*GT/Alg-ZnO beads have acquired higher thermal stability than both the CS*GT and CS*GT-ZnO beads. Figure 2C shows that, at 350 °C, CS/GT lost 50% of its initial weight (28%−78%) and CS/GT/ZnO lost 51% of its initial weight (39%−91%), while CS/GT*m-Alg/ZnO only lost 23% of its initial weight (50%−73%). The improvement in thermal stabilities can be attributed to the algae associated chemical components of the CS/GT*m-Alg/ZnO based on earlier studies.[38,39]

3.2. Adsorption Study. *3.2.1. Effect of Contact Time.* Figure 3A shows how the contact time affects the removal efficiency of BPA using CT/GT, CT/GT/ZnO, and CT/GT*m-Alg/ZnO beads through the presentation of the results of corresponding experiments. Various reaction times were implemented (10−60 min). The contact time at the beginning

https://doi.org/10.1021/acsomega.2c01985
ACS Omega 2022, 7, 27239−27248

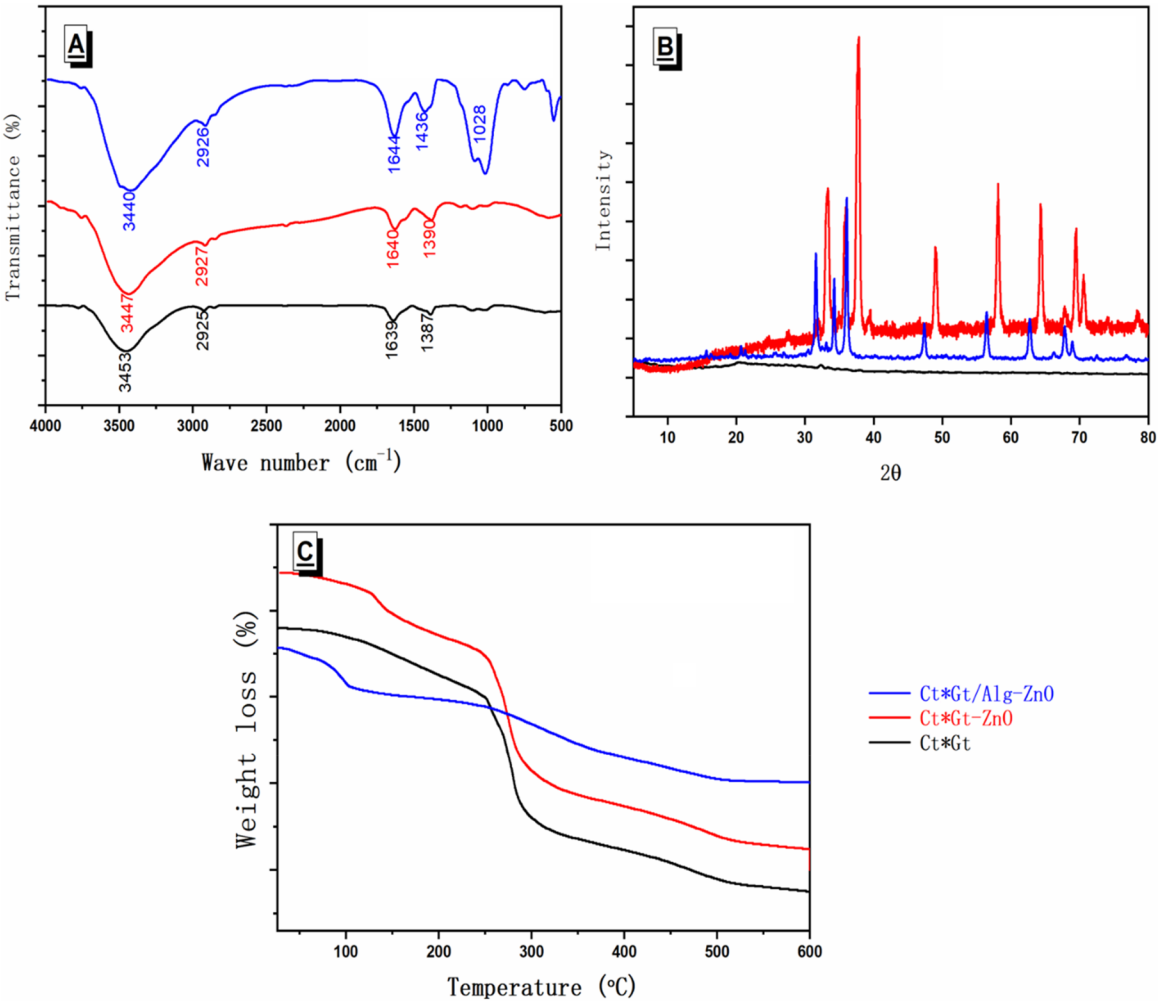

Figure 2. (A) FT-IR, (B) XRD, and (C) TGA analyses of CT/GT, CT/GT/ZnO, and CT/GT*m-Alg/ZnO beads.

was accomplished with removal efficiency because the sorbent active sites are still empty, causing the BPA molecules to be easily attached to the sorbent surface. An increase in the removal efficiency ability was established and observed from 1 to 20 min for BPA. The equilibrium conditions were obtained at 60 min.

3.2.2. Effect of pH. Acidity is an important factor because it affects the chemistry of the contaminants (i.e., hydrolysis, redox reactions, polymerization, and coordination). Acidity also has a strong influence on the ionic state of the active sites on the surface of adsorbents. The removal efficiency of BPA ions by CT/GT, CT/GT/ZnO, and CT/GT*m-Alg/ZnO sorbents was detected under different pH values. The experiments were performed at different pH values from 2 to 9 of BPA solution with equilibrium time 40 min. As shown in Figure 3B, the removal efficiency increased remarkably at lower initial pH value. It was observed that the optimal pH for the different adsorbents is pH 4, and above this value, the adsorption decreases slightly. This dramatic behavior can be attributed to the fact that, at the acidic conditions, the amino group ($-NH_2$) of the chitosan binds with H^+ ions producing the $-NH_3^+$. Then an interaction occurs between the $-NH_3^+$ and the anion form of BPA due to the electrostatic attractions between the adsorbent's active sites and BPA. Then the removal efficiency of the sorbent beads decreased due to break up of OH^- ions with the active site of the adsorbents bringing a net negative charge of the BPA ions above this pH and the repulsion forces between the negatively charged BPA and the surface layer of the adsorbent, so it will become more complicated and the BPA uptake is reduced. Figure 3B is shows that CT/GT*m-Alg/ZnO has the highest removal performance between different adsorbents, which reached 90%, while the adsorbent CT*GT has the lowest BPA uptake (58.3%), which may be due to the various functional groups present on the CT/GT*m-Alg/ZnO surface. The results show that the optimal pH value is 4 to ensure the maximum removal efficiency.

3.2.3. Effect of Adsorbent Dose. Figure 3C illustrates the effect of adsorbent dosage on BPA. A decrease in the remediation value was noticed with a gradual increase in the dose from 0.05 to 0.15 g. The reason is due to the increase in the adsorbent concentration in solution, which in turn increases the surface area of the studied adsorbent and summation of available adsorption sites. However, at high dosages, the available BPA molecules are insufficient to completely fill all available adsorption sites, leading to an equilibrium and surface saturation (Figure 3C). Additionally, masking of adsorption sites may occur at high adsorbent doses, creating electrostatic repulsion charged functional groups. The CT/GT*m-Alg/ZnO embedded form recorded a 97.1% removal efficiency of BPA solution, corresponding to a 39.25 mg/g uptake capacity, while the ideal removal percentages of

https://doi.org/10.1021/acsomega.2c01985
ACS Omega 2022, 7, 27239−27248

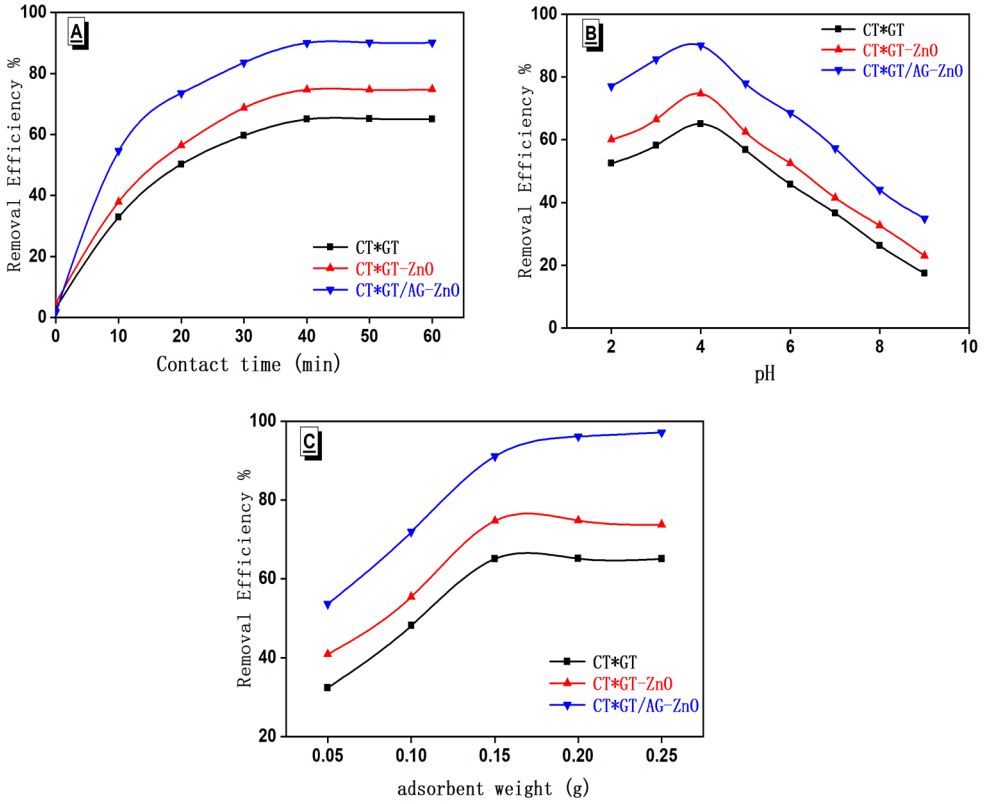

Figure 3. Effect of (A) contact time and (B and C) adsorbent weight on the removal efficiency of BPA by CT/GT, CT/GT/ZnO, and CT/GT*m-Alg/ZnO beads.

BPA onto CT/GT/ZnO adsorbents were 65.11% and 74.78%, respectively, corresponding to uptake capacities of 21.08 mg/g and 27.13 mg/g, respectively.

Marine algae are considered to be among the organisms that have a high capability of phytoremediation, especially *C. vulgaris*.[40] The results show that the optimal adsorbent dose is 0.15 g to ensure the maximum removal efficiency.

3.3. Adsorption Isotherms. The relationship between adsorption and adsorbate concentration can be described by isothermal models. The isotherm models Freundlich, Langmuir, and Temkin models had been used to fit the experimental data for BPA adsorbtion onto CT/GT, CT/GT/ZnO, and CT/GT*m-Alg/ZnO beads at room temperature. The Langmuir model describes the adsorption process as a unimolecular chemical combination, which occurs as a reversible reaction on a homogeneous/monolayer surface. The linear form of the Langmuir equation is given by the following:

$$C_e/q_e = 1/bq_m + C_e/q_m \quad (4)$$

where q_m (mg g^{-1}) represents the monolayer capacity and b (L mg^{-1}) represents the Langmuir constant. The C_e/q_e versus C_e plot shows a slope $1/q_m$ and intercept $1/bq_m$, as shown in Figure 4A. The calculated constants are given in Table 1. Upon inspection of Table 1, the correlation coefficients (R^2) for BPA were 0.996, 0.999, and 0.999 for CT/GT, CT/GT/ZnO, and CT/GT*m-Alg/ZnO, respectively, showing the applicability of the Langmuir model. The dimension separation factor, R_L, is given by eq 5:

$$R_L = 1/bC_0 \quad (5)$$

where b (L mg^{-1}) represents the Langmuir constant and the value of R_L indicates the isotherm to be either irreversible (R_L= 0), favorable ($0 < R_L < 1$), or unfavorable ($R_L > 1$). The R_L values for BPA adsorption onto CT/GT, CT/GT/ZnO, and CT/GT*m-Alg/ZnO composites were <1 and >0 to indicate favorable adsorption. The Freundlich model is applicable to study the adsorption of an adsorbate onto a multilayer surface of an adsorbent.

$$\ln q_e = \ln K_F + 1/n \ln C_e \quad (6)$$

where K_F (L mg^{-1}) represents the Freundlich constant and n represents heterogeneity factor, respectively. The Freundlich parameters were calculated from the linear plots of ln q_e versus ln C_e (Figure 4B). The Temkin model supposes that the adsorption heat would reduce linearly with the increase in coverage of the adsorbent. The isotherm is represented by the following:

$$q_e = (RT/b_T) \ln a_T + (RT/b_T) \ln C_e \quad (7)$$

$$q_e = B \ln a_T + B \ln C_e \quad (8)$$

$$B = RT/b_T \quad (9)$$

where q_e is the adsorbed amount at equilibrium, b_T (mg L^{-1}) is the Temkin isotherm constant, and a_T (L g^{-1}) is the binding constant. The heat adsorption values are listed in Table 1. The linearity of the Langmuir plots suggested that the adsorption processes by CT/GT, CT/GT/ZnO, and CT/GT*m-Alg/ZnO composites follow monolayer adsorption, which means that the adsorption sites are distributed homogeneously and the adsorption force is equivalent.

3.4. Kinetic Study. Figure 5 shows the adsorption kinetic models of CT/GT, CT/GT/ZnO, and CT/GT*m-Alg/ZnO, and Table 2 shows the fitting parameters. The pseudo-first-

https://doi.org/10.1021/acsomega.2c01985
ACS Omega 2022, 7, 27239−27248

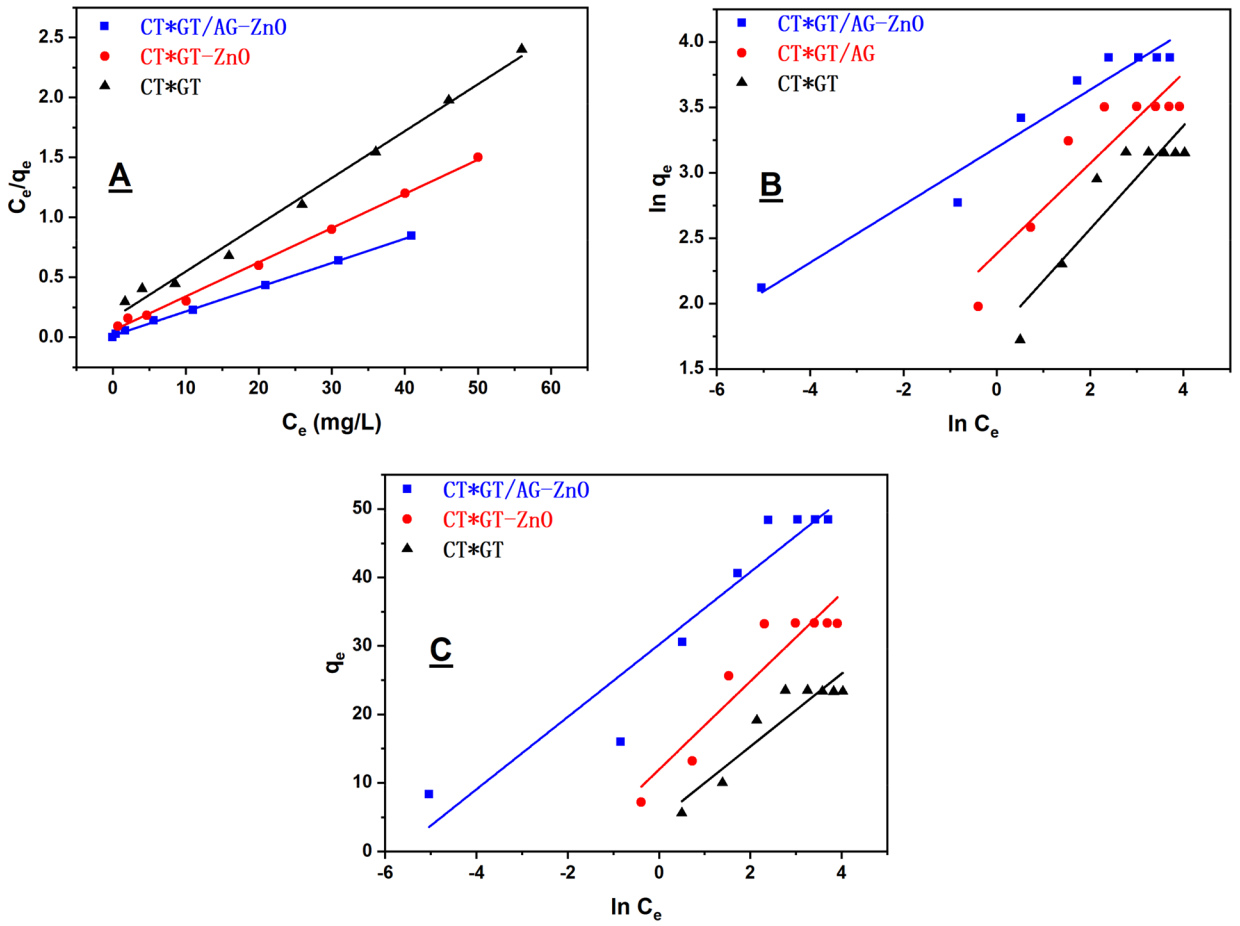

Figure 4. Isotherm models, (A) Langmuir, (B) Freundlich, and (C) Temkin, for BPA adsorption onto CT/GT, CT/GT/ZnO, and CT/GT*m-Alg/ZnO beads.

Table 1. Isotherm Parameters of BPA Adsorption onto CT/GT, CT/GT/ZnO, and CT/GT*m-Alg/ZnO Sorbents

	CT/GT/ST	CT/GT/ZnO	CT/GT*m-Alg/ZnO
q_e	20.18	27.34	39.07
Langmuir		$(C_e/q_e) = (1/q_{max})b + (C_e/q_{max})$	
R^2	0.996	0.999	0.999
q_{max}	20.08	25.98	38.24
B	1.51	1.89	2.24
Freundlich		$\ln q_e = \ln K_F + 1/n \ln C_e$	
R^2	0.947	0.944	0.948
q_m	10.35	14.74	22.06
K_f	0.137	0.229	0.423
Temkin		$q_e = B \ln a_T + B \ln C_e$	
R^2	0.961	0.965	0.957
a_T	1.73	2.658	6.32
B	1.32	1.36	1.54

order (PFO), pseudo-second-order (PSO), Elovich, and intraparticle diffusion (IPD) equations express the adsorption mechanism. A linear form of the pseudo-first-order model is as follows:

$$\ln(q_e - q_t) = \ln q_e - k_1 t \quad (10)$$

The k_1 values were calculated from ln $(q_e - q_t)$ versus t (Figure 5A), and q_e was calculated from the intercept. Table 2 shows the PFO constants. It indicates that adsorption of BPA onto different adsorbents does not follow pseudo-first-order kinetics due to the calculated correlation coefficient (R^2) being lower. The PSO model is expressed in eq 11:

$$t/q_t = 1/k_2 q_e^{\,2} + t/q_e \quad (11)$$

where K_2 (g mg^{-1} min^{-1}) is the rate constant of PSO adsorption. The linear plot of t versus t/q_t is shown in Figure 5B, and the calculated pseudo-second-order model is shown in Table 2. Elovich describes the heterogeneous surface and chemisorption kinetic applicability. The Elovich model is expressed by eq 12:

$$q_t = 1/\beta \ln \alpha\beta + 1/\beta \ln t \quad (12)$$

where α is the initial adsorption rate (mg g^{-1} min) and β is related to the extent of surface coverage and the activation energy for chemisorption. The correlation coefficients (R^2) were identified and are listed in Table 2. It is found that the correlation coefficient values of the PSO model for CT/GT, CT/GT/ZnO, and CT/GT*m-Alg/ZnO beads toward BPA are 0.994, 0.996, and 0.9999, respectively, indicating good linear plots. The q_e values calculated from the PSO model are close to those experimental values, indicating the applicability of the PSO mechanism for the adsorption of BPA onto CT/GT, CT/GT/ZnO, and CT/GT*m-Alg/ZnO sorbents.

We here show the intraparticle diffusion model of BPA ions into the surface of CT/GT*m-Alg/ZnO beads followed by interior pores via the IPD process, represented by equation 13:

https://doi.org/10.1021/acsomega.2c01985
ACS Omega 2022, 7, 27239−27248

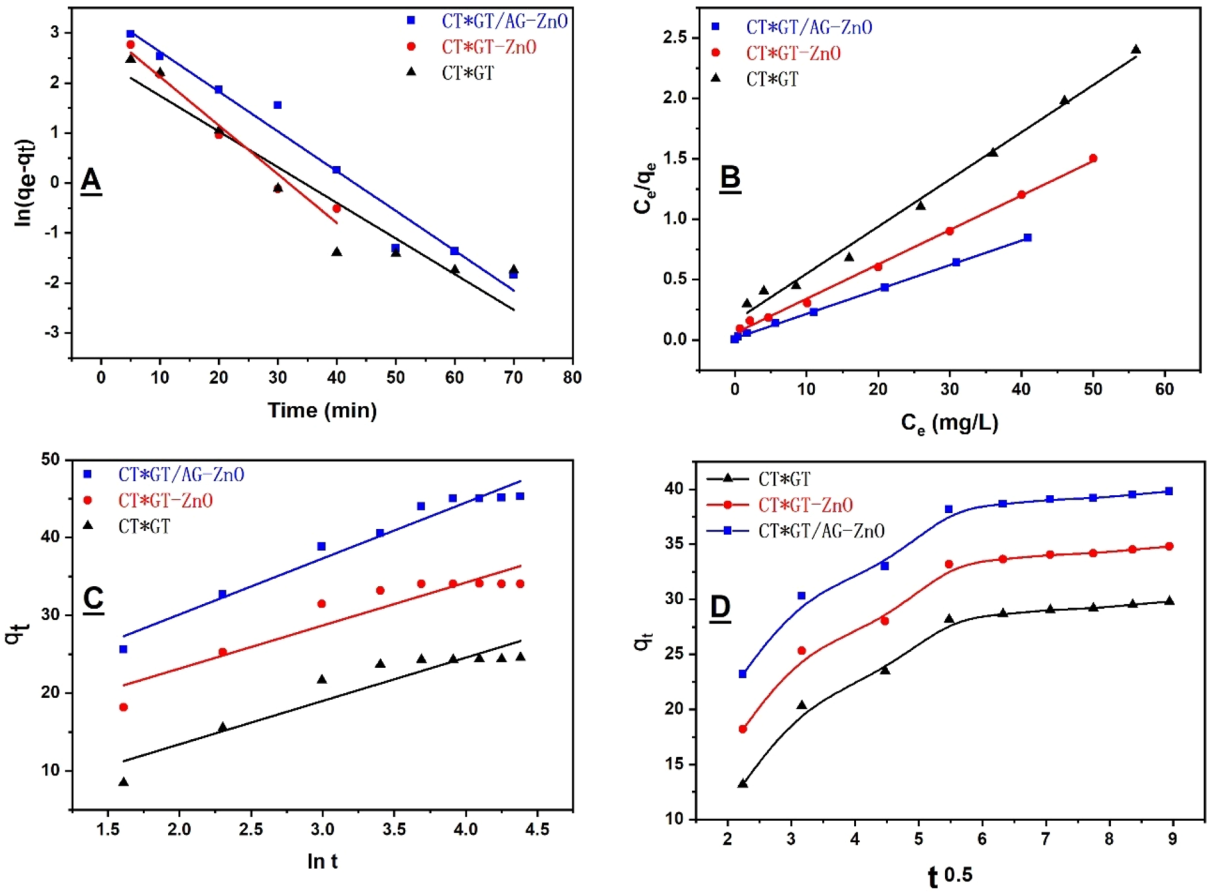

Figure 5. Kinetic models, (A) PFO, (B) PSO, (C) Elovich, and (D) IPD, for BPA adsorption onto CT/GT, CT/GT/ZnO, and CT/GT*m-Alg/ZnO sorbents.

Table 2. BPA Adsorption Kinetics onto CT/GT, CT/GT/ZnO, and CT/GT*m-Alg/ZnO Sorbents

	CT/GT/ST	CT/GT/ZnO	CT/GT*m-Alg/ZnO
PFO		$\ln(q_e - q_t) = \ln q_e - k_1 t$	
R^2	0.855	0.873	0.899
q_e	11.37	22.29	27.38
k_1	0.123	0.128	0.0419
PSO		$t/q_t = (1/k_2 q_e^2) + t/q_e$	
R^2	0.994	0.996	0.999
q_e	18.79	27.28	31.19
K_2	1.1×10^{-4}	1.2×10^{-4}	1.9×10^{-4}
Elovich		$q_t = \alpha + \beta \ln t$	
R^2	0.951	0.952	0.951
A	12.35	8.43	14.39
B	1.57	3.69	4.02
IPD		$q_t = k_i t^{1/2} + C$	
R^2	0.889	0.862	0.914
K_{id}	1.95	2.56	4.2
C	18.17	20.58	23.21

$$q_t = K_i t^{1/2} + C \quad (13)$$

In IPD, Ho shows q_t versus $t^{1/2}$ for intraparticle diffusion. The linearity of the plot shows BPA uptake into the beads. Here we show that IPD is involved in adsorption but is not the only rate-controlling step, proving a multistep adsorption process, onto the surface and into the interior. In Figure 5D, the adsorption follows an initial linear phase followed by a smooth curve showing a boundary layer effect followed by a second linear phase representing IPD. Table 2 shows that the driving forces depend on the adsorbate concentration. The BPA concentration correlates with the driving forces and diffusion rate. Additionally, the intercept correlates with the adsorption surface as the rate-limiting stage.

3.5. Regeneration. The effect of eluent on regeneration is investigated in Figure 6. NaOH reagent (0.5 M) was used for desorption of BPA from the aqueous solution. The regeneration efficiency was calculated from the desorption amount of BPA. To examine the stability of this adsorbent, adsorption−desorption cycles were examined. The CT/GT*m-Alg/ZnO composite (40 mg/50 mL) saturated with 40 mg L^{-1} of BPA was shaken at 140 rpm for 40 min. The adsorbent was precipitated and washed with distilled water. It is found that 88.62% of BPA was desorbed in 50 min using NaOH as adsorption medium (Figure 6A). It was illustrated that CT/GT*m-Alg/ZnO gave more than 90% removal of BPA up to 4 cycles followed by 52% efficiency decline after the fifth cycle (Figure 6B), indicating that the obtained adsorbent was found to have stable physical and chemical properties and be able to be regenerated for 4 times.

3.6. CT/GT*m-Alg/ZnO Adsorption Capacity. Table 3 shows the superior adsorption capacity of CT/GT*m-Alg/ZnO compared to previously reported formulas in addition to their high price or long treatments that limit their applications. Accordingly, CT/GT*m-Alg/ZnO is effective and cost-effective.

https://doi.org/10.1021/acsomega.2c01985
ACS Omega 2022, 7, 27239−27248

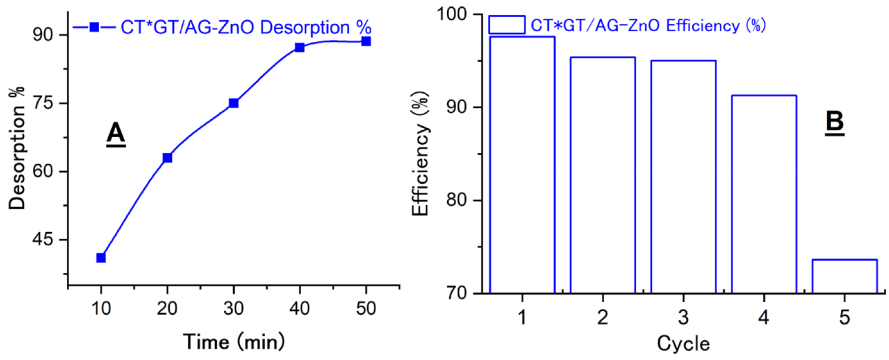

Figure 6. (A) BPA desorption and (B) reusability cycles of the CT/GT*m-Alg/ZnO composite for BPA adsorption at 40 min contact time, 40 mg/L BPA concentration, and 120 rpm agitation rate.

Table 3. Comparison of Adsorption Capacities of CT/GT*m-Alg/ZnO

Adsorbent	Adsorption capacity (mg/g)	Ref
Granulated activated carbon	16.26	41
Tea leaf waste	18.35	41
Barley husk	19.94	42
Commercial chitosan	27.02	43
Zeolite/β-cyclodextrin	32.7	44
CT/GT*m-Alg/ZnO	38.24	This study
TiO_2/polyethylene glycol diacrylate	101.4	45
Silica nanoparticles	155.78	46

4. CONCLUSION

A novel CT/GT*m-Alg/ZnO composite was successfully synthesized, characterized, and applied as an efficient agent for BPA removal from polluted water. The morphologies and textural properties of the newly synthesized CT/GT*m-Alg/ZnO nanocomposite adsorbent were identified by using FT-IR, SEM, and TGA. The results show that the developed CT/GT*m-Alg/ZnO had an adsorption capacity of 38.24 mg g^{-1} at pH 4. The results of the present work confirm that the incorporation of ZnO and microalgae into hydrogel beads leads to improvement of the adsorption capacity toward BPA disposable (38.24 mg g^{-1}). The adsorption study revealed that CT/GT*m-Alg/ZnO hydrogel composite is promising and has an excellent reusability performance after four cycles of removal of contaminants such as BPA from wastewater with low cost.

■ ASSOCIATED CONTENT

Supporting Information

The Supporting Information is available free of charge at https://pubs.acs.org/doi/10.1021/acsomega.2c01985.

Figure S1: GC chromatogram for the removal of BPA by CS/GT, CS/GT/ZnO, and CS/GT*m-Alg/ZnO beads (PDF)

■ AUTHOR INFORMATION

Corresponding Author

Mohamed R. El-Aassar − *Chemistry Department, College of Science, Jouf University, Sakaka 2014, Saudi Arabia;* orcid.org/0000-0002-9154-6089; Phone: +966547450636; Email: mrelaassar@ju.edu.sa

Authors

Hazim M. Ali − *Chemistry Department, College of Science, Jouf University, Sakaka 2014, Saudi Arabia*

Omar M. Ibrahim − *Department of Medicine, Washington University School of Medicine, St. Louis, Missouri 63110, United States;* orcid.org/0000-0002-9903-6657

Ahmed S. M. Ali − *Nuclear Power Plants Authority (NPPA), 11381 Cairo, Egypt*

Mahmoud A. Mohamed − *Polymer Materials Research Department Advanced Technology and New Material Institute, City of Scientific Research and Technological Applications (SRTA City), Alexandria 21934, Egypt*

Rehab Y. Ghareeb − *Department of Plant Protection and Bimolecular Diagnosis, Arid Lands Cultivation Research Institute (ALCRI), City of Scientific Research and Technological Applications (SRTA City), Alexandria 21934, Egypt*

Elsayed E. Hafez − *Department of Plant Protection and Bimolecular Diagnosis, Arid Lands Cultivation Research Institute (ALCRI), City of Scientific Research and Technological Applications (SRTA City), Alexandria 21934, Egypt*

Complete contact information is available at: https://pubs.acs.org/10.1021/acsomega.2c01985

Author Contributions

†H.M.A. and O.M.I. contributed equally to this work as first authors.

Notes

The authors declare no competing financial interest.

■ ACKNOWLEDGMENTS

This work was funded by the Deanship of Scientific Research at Jouf University under Grant No. DSR-2021-03-0347.

■ REFERENCES

(1) Pérez-Palacios, D.; Fernández-Recio, M. Á.; Moreta, C.; Tena, M. T. Determination of bisphenol-type endocrine disrupting compounds in food-contact recycled-paper materials by focused ultrasonic solid−liquid extraction and ultra performance liquid chromatography-high resolution mass spectrometry. *Talanta* **2012**, *99*, 167−174.

(2) La Merrill, M. A.; Vandenberg, L. N.; Smith, M. T.; Goodson, W.; Browne, P.; Patisaul, H. B.; Guyton, K. Z.; Kortenkamp, A.; Cogliano, V. J.; Woodruff, T. J. Consensus on the key characteristics of endocrine-disrupting chemicals as a basis for hazard identification. *Nat. Rev. Endocrinol.* **2020**, *16*, 45−47.

(3) Bhatnagar, A.; Anastopoulos, I. Adsorptive removal of bisphenol A (BPA) from aqueous solution: A review. *Chemosphere* **2017**, *168*, 885−902.
(4) Ibrahim, O. M.; Basse, P. H.; Jiang, W.; Guru, K.; Chatta, G.; Kalinski, P. NFκB-Activated COX2/PGE2/EP4 Axis Controls the Magnitude and Selectivity of BCG-Induced Inflammation in Human Bladder Cancer Tissues. *Cancers* **2021**, *13* (6), 1323.
(5) Ibrahim, O. M.; El-Deeb, N. M.; Abbas, H.; Elmasry, S. M.; El-Aassar, M. Alginate based tamoxifen/metal dual core-folate decorated shell: Nanocomposite targeted therapy for breast cancer via ROS-driven NF-κB pathway modulation. *Int. J. Biol. Macromol.* **2020**, *146*, 119−131.
(6) Ibrahim, O. M.; Pandey, R. K.; Chatta, G.; Kalinski, P. Role of tumor microenvironment in the efficacy of BCG therapy. *Trends in Research* **2020**, *3* (4), 1−3.
(7) Jin, F.-L.; Li, X.; Park, S.-J. Synthesis and application of epoxy resins: A review. *J. Ind. Eng. Chem.* **2015**, *29*, 1−11.
(8) El-Aassar, M.; Alsohaimi, I. H.; Ali, A. S.; Elzain, A. A. Removal of phenol and Bisphenol A by immobilized Laccase on poly (Acrylonitrile-co-Styrene/Pyrrole) nanofibers. *Sep. Sci. Technol.* **2020**, *55*, 2670−2678.
(9) Snoj-Tratnik, J.; Kosjek, T.; Heath, E.; Mazej, D.; Ćehić, S.; Karakitsios, S. P.; Sarigiannis, D. A.; Horvat, M. Urinary bisphenol A in children, mothers and fathers from Slovenia: Overall results and determinants of exposure. *Environ. Res.* **2019**, *168*, 32−40.
(10) Huang, Y.; Wong, C.; Zheng, J.; Bouwman, H.; Barra, R.; Wahlström, B.; Neretin, L.; Wong, M. H. Bisphenol A (BPA) in China: a review of sources, environmental levels, and potential human health impacts. *Environ. Int.* **2012**, *42*, 91−99.
(11) Zhu, Y.; Zhu, R.; Xi, Y.; Xu, T.; Yan, L.; Zhu, J.; Zhu, G.; He, H. Heterogeneous photo-Fenton degradation of bisphenol A over Ag/AgCl/ferrihydrite catalysts under visible light. *Chem. Eng. J.* **2018**, *346*, 567−577.
(12) Tan, X.; Wan, Y.; Huang, Y.; He, C.; Zhang, Z.; He, Z.; Hu, L.; Zeng, J.; Shu, D. Three-dimensional MnO2 porous hollow microspheres for enhanced activity as ozonation catalysts in degradation of bisphenol A. *J. Hazard. Mater.* **2017**, *321*, 162−172.
(13) Yu, L.; Wang, C.; Ren, X.; Sun, H. Catalytic oxidative degradation of bisphenol A using an ultrasonic-assisted tourmaline-based system: Influence factors and mechanism study. *Chem. Eng. J.* **2014**, *252*, 346−354.
(14) Al-Musawi, T. J.; Mengelizadeh, N.; Ganji, F.; Wang, C.; Balarak, D. Preparation of multi-walled carbon nanotubes coated with $CoFe_2O_4$ nanoparticles and their adsorption performance for Bisphenol A compound. *Adv. Powder Technol.* **2022**, *33* (2), 103438.
(15) Balarak, D.; Mostafapour, F. K.; Lee, S. M.; Jeon, C. Adsorption of bisphenol a using dried rice husk: equilibrium, kinetic and thermodynamic studies. *Appl. Chem. Eng.* **2019**, *30* (3), 316−323.
(16) Mohammadi, L.; Bazrafshan, E.; Noroozifar, M.; Ansari-Moghaddam, A.; Barahuie, F.; Balarak, D. Removing 2, 4-dichlorophenol from aqueous environments by heterogeneous catalytic ozonation using synthesized MgO nanoparticles. *Water Sci. Technol.* **2017**, *76* (11), 3054−3068.
(17) Tuzen, M.; Sarı, A.; Saleh, T. A. Response surface optimization, kinetic and thermodynamic studies for effective removal of rhodamine B by magnetic AC/CeO_2 nanocomposite. *J. Environ. Manage.* **2018**, *206*, 170−177.
(18) Altintig, E.; Onaran, M.; Sarı, A.; Altundag, H.; Tuzen, M. Preparation, characterization and evaluation of bio-based magnetic activated carbon for effective adsorption of malachite green from aqueous solution. *Mater. Chem. Phys.* **2018**, *220*, 313−321.
(19) Zhang, Y.; Cui, W.; An, W.; Liu, L.; Liang, Y.; Zhu, Y. Combination of photoelectrocatalysis and adsorption for removal of bisphenol A over TiO2-graphene hydrogel with 3D network structure. *Appl. Catal. B: Environ.* **2018**, *221*, 36−46.
(20) Dehghani, M. H.; Ghadermazi, M.; Bhatnagar, A.; Sadighara, P.; Jahed-Khaniki, G.; Heibati, B.; McKay, G. Adsorptive removal of endocrine disrupting bisphenol A from aqueous solution using chitosan. *J. Environ. Chem. Eng.* **2016**, *4* (3), 2647−2655.
(21) Luo, Y.; Wang, Q. Recent development of chitosan-based polyelectrolyte complexes with natural polysaccharides for drug delivery. *Int. J. Biol. Macromol.* **2014**, *64*, 353−367.
(22) Kaur, S.; Dhillon, G. S. The versatile biopolymer chitosan: potential sources, evaluation of extraction methods and applications. *Crit. Rev. Microbiol.* **2014**, *40* (2), 155−175.
(23) Baroni, P.; Vieira, R.; Meneghetti, E.; Da Silva, M.; Beppu, M. Evaluation of batch adsorption of chromium ions on natural and crosslinked chitosan membranes. *J. Hazard. Mater.* **2008**, *152* (3), 1155−1163.
(24) El-Aassar, M.; Ibrahim, O. M.; Fouda, M. M.; Fakhry, H.; Ajarem, J.; Maodaa, S. N.; Allam, A. A.; Hafez, E. E. Wound dressing of chitosan-based-crosslinked gelatin/polyvinyl pyrrolidone embedded silver nanoparticles, for targeting multidrug resistance microbes. *Carbohydr. Polym.* **2021**, *255*, 117484.
(25) El-Aassar, M.; Ibrahim, O. M.; Fouda, M. M.; El-Beheri, N. G.; Agwa, M. M. Wound healing of nanofiber comprising Polygalacturonic/Hyaluronic acid embedded silver nanoparticles: In-vitro and in-vivo studies. *Carbohydr. Polym.* **2020**, *238*, 116175.
(26) El-Aassar, M.; Ibrahim, O. M.; Al-Oanzi, Z. H. Biotechnological Applications of Polymeric Nanofiber Platforms Loaded with Diverse Bioactive Materials. *Polymers* **2021**, *13* (21), 3734.
(27) Yan, X.; Yi, C.; Wang, Y.; Cao, W.; Mao, D.; Ou, Q.; Shen, P.; Wang, H. Multi-catalysis of nano-zinc oxide for bisphenol A degradation in a dielectric barrier discharge plasma system: Effect and mechanism. *Sep. Purif. Technol.* **2020**, *231*, 115897.
(28) Agarwal, H.; Venkat Kumar, S.; Rajeshkumar, S. A review on green synthesis of zinc oxide nanoparticles−An eco-friendly approach. *Resource-Efficient Technologies* **2017**, *3* (4), 406−413.
(29) Ji, M.-K.; Kabra, A. N.; Choi, J.; Hwang, J.-H.; Kim, J. R.; Abou-Shanab, R. A. I.; Oh, Y.-K.; Jeon, B.-H. Biodegradation of bisphenol A by the freshwater microalgae Chlamydomonas mexicana and Chlorella vulgaris. *Ecol. Eng.* **2014**, *73*, 260−269.
(30) El-Deeb, N. M.; Abo-Eleneen, M. A.; Al-Madboly, L. A.; Sharaf, M. M.; Othman, S. S.; Ibrahim, O. M.; Mubarak, M. S. Biogenically Synthesized Polysaccharides-Capped Silver Nanoparticles: Immunomodulatory and Antibacterial Potentialities Against Resistant Pseudomonas aeruginosa. *Front. Bioeng. Biotechnol.* **2020**, *8*, 643 DOI: 10.3389/fbioe.2020.00643.
(31) Hirooka, T.; Nagase, H.; Uchida, K.; Hiroshige, Y.; Ehara, Y.; Nishikawa, J. i.; Nishihara, T.; Miyamoto, K.; Hirata, Z. Biodegradation of bisphenol A and disappearance of its estrogenic activity by the green alga Chlorella fusca var. vacuolata. *Environ. Toxicol. Chem.* **2005**, *24* (8), 1896−1901.
(32) Mohan, A. C.; Renjanadevi, B. Preparation of zinc oxide nanoparticles and its characterization using scanning electron microscopy (SEM) and X-ray diffraction (XRD). *Procedia Technology* **2016**, *24*, 761−766.
(33) El-Deeb, N. M.; Ibrahim, O. M.; Mohamed, M. A.; Farag, M. M.; Farrag, A. A.; El-Aassar, M. Alginate/κ-carrageenan oral microcapsules loaded with Agaricus bisporus polysaccharides MH751906 for natural killer cells mediated colon cancer immunotherapy. *Int. J. Biol. Macromol.* **2022**, *205*, 385−395.
(34) Shibraen, M. H.; Ibrahim, O. M.; Asad, R. A.; Yang, S.; El-Aassar, M. Interpenetration of metal cations into polyelectrolyte-multilayer-films via layer-by-layer assembly: Selective antibacterial functionality of cationic guar gum/polyacrylic acid-Ag+ nanofilm against resistant E. coli. *Colloids Surf. A Physicochem. Eng.* **2021**, *610*, 125921.
(35) Morais, F. P.; Simões, R. M. S.; Curto, J. M. R. Biopolymeric Delivery Systems for Cosmetic Applications Using Chlorella vulgaris Algae and Tea Tree Essential Oil. *Polymers* **2020**, *12* (11), 2689.
(36) Ludi, B.; Niederberger, M. Zinc oxide nanoparticles: chemical mechanisms and classical and non-classical crystallization. *Dalton Trans.* **2013**, *42* (35), 12554−12568.
(37) Uikey, P.; Vishwakarma, K. Review of zinc oxide (ZnO) nanoparticles applications and properties. *IJETCSE* **2016**, *21* (2), 239−242.

https://doi.org/10.1021/acsomega.2c01985
ACS Omega 2022, 7, 27239−27248

(38) Robal, M.; Truus, K.; Volobujeva, O.; Mellikov, E.; Tuvikene, R. Thermal stability of red algal galactans: Effect of molecular structure and counterions. *Int. J. Biol. Macromol.* **2017**, *104*, 213−223.
(39) Bhola, V.; Desikan, R.; Santosh, S. K.; Subburamu, K.; Sanniyasi, E.; Bux, F. Effects of parameters affecting biomass yield and thermal behaviour of Chlorella vulgaris. *J. Biosci. Bioeng.* **2011**, *111* (3), 377−382.
(40) Chin, J. Y.; Chng, L. M.; Leong, S. S.; Yeap, S. P.; Yasin, N. H. M.; Toh, P. Y. Removal of synthetic Dye by Chlorella vulgaris microalgae as natural adsorbent. *Arabian J. Sci. Eng.* **2020**, *45* (9), 7385−7395.
(41) Ifelebuegu, A.; Ukpebor, J.; Obidiegwu, C.; Kwofi, B. Comparative potential of black tea leaves waste to granular activated carbon in adsorption of endocrine disrupting compounds from aqueous solution. *Global J. Environ. Sci. Manag.* **2015**, *1* (3), 205−214.
(42) Balarak, D. Kinetics, isotherm and thermodynamics studies on bisphenol A adsorption using barley husk. *Int. J. ChemTech Res.* **2016**, *9* (5), 681−690.
(43) Kyzas, G. Z.; Bikiaris, D. N.; Lambropoulou, D. A. Effect of humic acid on pharmaceuticals adsorption using sulfonic acid grafted chitosan. *J. Mol. Liq.* **2017**, *230*, 1−5.
(44) Bandura, L.; Białoszewska, M.; Malinowski, S.; Franus, W. Adsorptive performance of fly ash-derived zeolite modified by β-cyclodextrin for ibuprofen, bisphenol A and caffeine removal from aqueous solutions−equilibrium and kinetic study. *Appl. Surf. Sci.* **2021**, *562*, 150160.
(45) Piao, M.; Du, H.; Sun, Y.; Teng, H. Self-regeneration hybrid hydrogel for bisphenol a adsorption in water. *Environmental Science and Pollution Research International* **2022**, *29*, 43169−43178.
(46) Rovani, S.; Santos, J. J.; Guilhen, S. N.; Corio, P.; Fungaro, D. A. Fast, efficient and clean adsorption of bisphenol-A using renewable mesoporous silica nanoparticles from sugarcane waste ash. *RSC Adv.* **2020**, *10* (46), 27706−27712.

https://doi.org/10.1021/acsomega.2c01985
ACS Omega 2022, 7, 27239−27248